

# INTEGRATION OF A TERRESTRIAL LIDAR ON A MOBILE MAPPING PLATFORM: FIRST EXPERIENCES

M. Alshawa, E. Smigiel, P. Grussenmeyer, T. Landes

<sup>a</sup> Photogrammetry and Geomatics Group MAP-PAGE UMR 694, Graduate School of Science and Technology (INSA),  
24 Boulevard de la Victoire, 67084 STRASBOURG, France  
(majd.alshawa, eddie.smigiel, pierre.grussenmeyer, tania.landes)@insa-strasbourg.fr

**KEY WORDS:** experiment, TLS, GPS/INS, integration, modelling, error, accuracy.

## ABSTRACT:

Mobile mapping techniques represent an efficient way to supply the requirements imposed by the development of 3D GIS, urban digital models and their applications using virtual and augmented reality. The methods widely applied in this domain depend on the video and photogrammetric sensors which provide accurate results but with long time of post-processing. Hence, the integration of a terrestrial laser scanner or terrestrial LiDAR in such mobile mapping platforms would allow obtaining point cloud quickly at low operating cost. However this technique requires an ideal synchronisation between the different components. Each laser pulse has to be strictly synchronized with the GPS/INS module which enables to establish the trajectory of the platform. Terrestrial Laser Scanners (TLS), though, mostly designed for static stations, usually do not give the exact time of each laser pulse. In this paper, we show that under some conditions, it is possible to synchronize point cloud obtained by the TLS with the trajectometry data, in order to achieve the georeferencing of the scanned cloud points into a world coordinate system. We describe the error model and accuracy that one can reach with such a platform, and we illustrate the theoretical results with experimental data obtained by a platform prototype developed at the MAP-PAGE laboratory at INSA of Strasbourg. Thus, we demonstrate that a terrestrial vehicle-borne LiDAR technique can be considered as a novel alternative for the traditional mapping methods.

## 1. INTRODUCTION

Mobile Mapping System (MMS) has come to light since a decade of years as a low-cost surveying method. It has been applied in many domains such as road-mapping, culture heritage and architectural survey. It stands for a principal resource of road cadastre, 3D GIS, creating accurate virtual environments and the augmented reality models. The external absolute systems of localization (GPS for example) and the dead reckoning navigation (INS or odometer) have many complementary characters. Their intergration makes dynamic localisation a simple mission especially in urban areas. The early applications were limited to close range land photogrammetry because of the reduction (or avoidance) of the huge exterior orientation calculations. It employs photogrammetric cameras as mapping sensors, where each camera embedded in the system is therefore georeferenced in the global frame from the positional data acquired by the GPS/INS system (georeferencing sensor). INS gives also data for the exterior orientation of the cameras. The second generation of MMS uses laser scanners instead of the photogrammetric cameras or combines both. Usually, line-scanners are used to cover the whole scene during the displacement. Traditional (MMS) systems work with forward-, backward-, or side-looking sensors (Zhao and Shibasaki, 2001; Abuhadrous and al. 2004).

However, Terrestrial Laser Scanners (TLSs) are rarely used or adapted for mobile mapping system, so a little related work can be found for this usage. In our paper, we discuss the precision of a TLS mobile mapping system, we will revise error navigation model, laser scan error model and how the two models will contribute in the final accuracy model of the resulted point cloud.

A lack of exhaustive error model study in the domain of mobile mapping laser system can be noticed in the related literature, nevertheless one can find important error analysis in the domain of airborne laser scanning in some approaches such as (Baltsavias,1999).

We will firstly introduce our prototype of a mobile system based on a TLS, then we provide a review of all system errors and we present briefly the principles of INS/GPS navigation, Kalman filter and related accuracy issues. Thereafter we focus on LiDAR errors model and their propagation in order to represent a final model of LiDAR-navigation errors estimation. Even though the work presented here is still "in progress", we are able to present some first reconstruction results at the end of this article.

## 2. EXPERIMENT DESCRIPTION AND SYSTEM CONFIGURATION

Our prototype consists of three main components: GPS/INS/TLS mounted on a trailer which can be drawn by human force or by a land vehicle according to the situation (see Figure 1). The major characteristics for each element are:

- GPS: Leica® GPS1200 working in differential mode, the sampling rate used was uniformed at 1-2 Hz
- INS: AP04 of UAV® navigation auto-pilot unit from which we used only the INS measurements. The accelerometer bias standard is  $\pm 0.3$  m/s<sup>2</sup> and the standard noise is  $\pm 0.2$  m/s<sup>2</sup> at 100 Hz while bias standard of gyrometer is  $\pm 0.5$  deg/sec and its standard noise is equal to  $\pm 0.1$  deg/sec at 100 Hz too.
- TLS: laser scanner 3D GX DR 200+ from Trimble® which will replace the usual 2D scanner. Thus it will be interesting to know some of its common 2D/3D technical specifications such as the range of laser which can reach 200m and the maximum vertical field of view which is 60 deg. The last calibration yields a distance accuracy of 7 mm at 100 m and an angle accuracy of 12"-14" while measuring a single point.

Since the AP04 can be linked to a GPS antenna and can operate its measurement, it provides normally the UTC time of day for each packet of INS measurement. Thus, the synchronisation between the used GPS and INS should not

cause any problem. PointScope®, the software which operates the scanner, enables to know the scan starting time and its duration. The recorded time is provided by the computer clock. Hence, the synchronisation between the computer-time and the GPS-time is possible by the synchronisation between their clocks and by using GPS-time, ATI-time, and UTC-time conversion laws.

In order to exploit the system measurements, we develop herein on the one hand, all the required observation equations. On the other hand, we highlight the errors related to each component of the system, as well as their effects on the final coordinate calculations.



Figure 1. The current setup of our mobile platform

The error of synchronization has the most important contribution in the final point cloud accuracy. It may cause unexpected shift or rotation in such a way that the awaited corrections play the part of additional errors. The synchronisation is often achieved by specific electronics; therefore this error will not be developed in this approach, though in the present conditions of the herein described experiments it should not be neglected.

### 3. MEASUREMENT ERROR SOURCES AND MODELING:

Since our MMS system depends on the navigation component INS/GPS, we can state three sources of errors: GPS errors, INS error and TLS error. All errors resulting from lever arm and orientation measurement between the elements of the triple GPS/INS/TLS will be determined in the static calibration stage. They will be treated as time-invariant systematic errors to be omitted before starting the dynamic stage. The latter calibration enables to define completely the transformation between the body/sensor/platform frames explained later.

#### 3.1 GPS error

A number of conditions can reduce the accuracy of a GPS receiver, the effect of these factors can be expressed as pseudo-range model, especially since a tightly coupled Kalman filter will be detailed later. GPS pseudo-range measurements  $\rho$  are noisy estimates of the range ( $r$ ) from satellite to receiver. Pseudo-range values are available from code and carrier phase measurements. The model for code pseudo-range measurements is (Rankin, J., 1994):

$$\rho_{code} = r + \delta_{eph} + \delta_{iono} + \delta_{tropo} + \delta_{SA} - cT + \delta_{mp} + v_{rcvr} \quad (1)$$

With  $\delta_{eph}$ : satellite ephemeris error  
 $\delta_{iono}$ : ionosphere error  
 $\delta_{tropo}$ : troposphere error  
 $\delta_{SA}$ : Selective Availability (SA) error

$c$ : speed of light  
 $T$ : receiver clock error  
 $\delta_{mp}$ : multipath error  
 $v_{rcvr}$ : receiver measurement noise

The model for the L-band carrier phase measurement has similar error terms as the code pseudo-range except that ionospheric delay is negative for phase and positive for code.

After multiplying by the carrier wavelength  $\lambda$ , the carrier phase model (in meters) is:

$$\lambda\phi = r + \delta_{eph} + \delta_{iono} + \delta_{tropo} + \delta_{SA} - cT + \delta_{mp} + v_{rcvr} + \lambda N \quad (2)$$

Where:  $N$  represents the integer ambiguity

The above errors can be characterized by an appropriate error model as random walk or Gauss- Markov processes.

### 3.2 INS Errors

#### 3.2.1 INS Error sources and modeling

Most of the error sources that corrupt the navigation solution are sensor errors or random disturbances (Stovall, 1997). The common errors in sensor level (or sensor space) for a strapdown INS (used in the majority of modern navigation systems) are:

- Bias errors: a constant signal on the output of a sensor, independent of the input. A bias will not change during a run, but may vary from turn-on to turn-on. These errors are only constant for short terms, and they typically exhibit drift that might be modeled usually by first-order Gauss-Markov processes;
- Scale factor errors: a linear error that is proportional to the input signal. Scale factor is usually specified in parts per million (ppm);
- Alignment errors: roll, pitch and yaw angle errors caused by the misalignment with the body of the navigation frame.

Other error sources are nonlinearity, acceleration sensitivity, g-sensitivity and quantization error in all digitized systems. The deterministic part of accelerometer and gyro sensor errors, including biases and scale factors, can be determined by calibration and then removed from the raw measurements. The stochastic part, due to the variations in the INS sensor bias terms, represents the residual biases and hence, will be modeled stochastically to be included in the INS error model.

In order to express the latter errors in the state space, one must know that INS has two phase operations: the alignment phase and the navigation phase. The navigation phase starts from the initial velocity, position and attitude, while process for determining these INS initial conditions is called alignment. Any error in either phase will be integrated and will propagate over time.

Strapdown INS navigation computation equations (mechanization) can be written in various coordinate systems. The way of writing the differential equations of the system in the form of a set of first order equation and latterly its perturbation (error propagation) generate many forms of error models. The INS error equations correspondently can be written also in different frames. The most commonly used error equations are expressed in the c-frame, which is the so-called psi-angle model, or in the true frame which is so called phi-angle (Benson, 1975). Other approaches (Kong, 2004) use quaternions to express psi-angle model. These models are used widely in the GPS/INS integration Kalman filter. For instance, the psi-angle model, for the Position, Velocity and Attitude

(PVA) respectively errors, given by (Bar-Itzhack and Breman, 1988) are:

$$\begin{aligned} \delta \mathbf{r} &= -\omega_{en}^c \times \delta \mathbf{r}^c + \delta \mathbf{v}^c \\ \delta \mathbf{v}^c &= -(\omega_{ie}^c + \omega_{in}^c) \times \delta \mathbf{v} - \delta \boldsymbol{\psi} \times \mathbf{f} + \nabla + \delta \mathbf{g}^c \end{aligned} \quad (3)$$

$$\delta \boldsymbol{\psi} = -\omega_{in}^c \times \delta \boldsymbol{\psi} + \boldsymbol{\varepsilon}$$

where:

$\nabla$  : the accelerometer error vector

$\boldsymbol{\varepsilon}$  : the gyro drift error

$\delta \mathbf{g}$  : the gravity anomaly vector

$\mathbf{f}$  : the specific force vector sensed by accelerometer

$\omega_{kl}^j$  : angular rate between  $k$  and  $l$ -frame resolved in  $j$ -frame.

$c, e, i, n$  : computer, earth, inertial and navigation frames respectively.

Both accelerometer bias and gyro drift are modelled as first order Gauss-Markov processes. One can get a state vector by adding accelerometer bias and gyro drift to PVA inertial vector, so that:

$$\dot{\mathbf{x}} = \begin{pmatrix} \delta \mathbf{r} & \delta \mathbf{v} & \delta \boldsymbol{\psi} & \dot{\nabla} & \boldsymbol{\varepsilon} \end{pmatrix}^T \quad (4)$$

This 15-states vector is adjusted through the Kalman filter evoked in the next paragraph.

### 3.2.2 INS/GPS Kalman filter design

Various forms of INS/GPS integration techniques have been developed in the literature ((Kong 2004), (Wang et al, 2003)). Kalman filtering is still one of the most suitable integration techniques to combine the inertial and GPS measurement. Nevertheless it requires adequate dynamics measurement covariance model for both of GPS, INS systems.

The Kalman filter provides usually the covariance matrix  $P_K$  of the state vector  $\dot{\mathbf{x}}$  in each INS sampling moments. This matrix is needed when computing the final error model, but after adding additional terms of error resulting of TLS for which the next paragraph is devoted.

### 3.3 TLS errors

As mentioned in the introduction, scanners usually used by MMS are line scanners which depend on propagation delay of a laser beam (time of flight). In our experiment, we use a TLS which is supposed to work as a stationary scanner. It has been adapted to mobile sessions with some limitations. Indeed, it is impossible to scan both road sides in one time since the vertical field of view is limited.

Obviously the systematic errors of the scan have to be eliminated before any measurement. (Lichti and Licht, 2006) classified the systematic errors into two groups: systematic and physical error. The systematic errors contribute by 19 coefficients of self calibration calculation: 8 for range, 7 for horizontal direction and 4 for elevation angle. Then the physical intervention on wavelength was expressed by two sets of cyclic error terms.

Nevertheless, for the purpose of our study, we will adopt the classification pointed out by (Reshetyuk, 2006) since it underlines the influence of scanned object on the final accuracy of the point cloud. Hence, scanning errors are expressed in three major groups as follows:

1. Instrumental systematic errors: these errors vary from a scanner to another according to device design and the manufacture imperfection. Range measurement in time-of-flight scanners is affected by a set of errors like the random jitter, walk time, non linearity, temperature

interior drift, zero error, scale error and mixed pixel. We will refer to the instrumental range error and accuracy by  $\Delta r_{inst}, \sigma_{r_{inst}}$  respectively. More details can be found in (Reshetyuk, 2006). Angles are also affected by other categories of errors which depend on the mechanical arrangement of scanner rotating mirror (flat, polygonal, or oscillating). These errors can be summarized by mirror surface roughness and gradual erosion, velocity variation, zero error and scale error. The third category which can be added is the vertical, horizontal, mirror and collimation axe error. Estimation of systematic instrumental errors mentioned above is the task of laser scanner calibration by the manufacturer;

2. Object related errors: these errors are related to reflectance properties of object surface due to several factors as material properties, laser wavelength, polarization, and surface colour, moisture, roughness and temperature;

3. Environmental errors which affect the laser beam propagation in the atmosphere, causing both distortion and attenuation of returned signal. The degree of attenuation depends on the wavelength, temperature, pressure, microscopic particles in the air and weather conditions. Other factors influencing laser beam propagation are reflection and atmospheric turbulence, due to the beam wander from its initial direction and Gaussian wavefront distortion called beam intensity fluctuation. We can find in the literature many empirical models trying to model these effects.

Even after correcting angles and range for all significant systematic errors, we can keep a component  $\Delta r_{inst}$  in our model due to random errors. The object-related errors could be simplified to an offset  $\Delta r_{reflect}$ , and  $\Delta r_{mult.ret}$  resulting from multiple returns, while the environmental one can be written as  $\Delta r_{ref.ind}$  which reflects the velocity correction due to reflectance index change.

Finally the correction on range measured will be:

$$\Delta r_{corr} = -\Delta r_{inst} - \Delta r_{reflect} + \Delta r_{ref.ind} - \Delta r_{mult.ret} \quad (5)$$

The total range accuracy may be computed as follows:

$$\sigma_{corr}^2 = \sigma_{inst}^2 + \sigma_{reflect}^2 + \sigma_{ref.ind}^2 + \sigma_{mult.ret}^2 \quad (6)$$

Equation (6) means that all the cross correlation (covariance) terms between error factors have been neglected.

The error in vertical angle measurement is given by :

$$\Delta \theta = -(\theta_0 + \theta_{scan}) \delta \theta \quad (7)$$

where  $\theta_0, \delta \theta$  are resp. the vertical index and scale error.

The accuracy of the corrected vertical angle is:

$$\sigma_{\theta_{corr}}^2 = \sigma_{\theta}^2 + \sigma_{\theta_0}^2 + \theta_{scan}^2 \sigma_{\delta \theta}^2 \quad (8)$$

$\sigma_{\theta}$  is the vertical angle noise which can be determined by the characteristics of the angular position sensor.

The determination of the horizontal angular accuracy is not important for 2D line scanners, but for 3D line scanners it is given by:

$$\Delta \varphi = \left( \frac{c}{\cos \theta_{scan}} + i \cdot \tan \theta_{scan} \right) \quad (9)$$

$$\sigma_{\varphi_{coord}} = \sigma_{\varphi}^2 + \frac{\sigma_c^2}{\cos^2 \theta_{scan}} + \tan^2 \theta_{scan} \cdot \sigma_i^2 \quad (10)$$

Where  $c$  and  $i$  are collimation and horizontal axis errors, respectively.

#### 4. INS/GPS/TLS ERROR MODEL

In order to simplify the error model, the perturbations of scanner position and attitude are supposed to remain constant during the time between two consecutive scanned points. Hence we can consider our model as a discrete one (considering discrete as a language convenience).

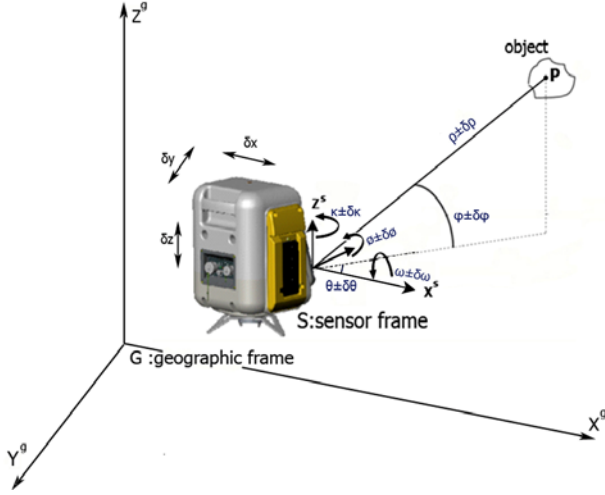


Figure 2. Schema of a perturbed scanner in geographic space

Figure 2 illustrates the perturbed sensor-frame in a local geographic frame. For a scanned point  $P$ , following equations can be established:

$$\begin{pmatrix} x_p^g \\ y_p^g \\ z_p^g \end{pmatrix} = \begin{pmatrix} x_s^g \\ y_s^g \\ z_s^g \end{pmatrix} + C_s^g \begin{pmatrix} x_p^s \\ y_p^s \\ z_p^s \end{pmatrix} = \begin{pmatrix} x_s^g \\ y_s^g \\ z_s^g \end{pmatrix} + C_s^g \rho \begin{pmatrix} \cos \phi \cos \theta \\ \cos \phi \sin \theta \\ \sin \phi \end{pmatrix} \quad (11)$$

Or in another way:

$$\begin{aligned} x_p^g &= x_s^g + c_{11}x_p^s + c_{12}y_p^s + c_{13}z_p^s \\ y_p^g &= y_s^g + c_{21}x_p^s + c_{22}y_p^s + c_{23}z_p^s \\ z_p^g &= z_s^g + c_{31}x_p^s + c_{32}y_p^s + c_{33}z_p^s \end{aligned} \quad (12)$$

where:

$\begin{pmatrix} x_p^g & y_p^g & z_p^g \end{pmatrix}^T$ : coordinates of a point  $P$  in the point cloud

$\begin{pmatrix} x_s^g & y_s^g & z_s^g \end{pmatrix}^T$ : scanner position in the geographic frame

$C_s^g$ : DCM (Direction Cosine Matrix) from sensor frame to geographic frame whose elements are  $C_{ij}$ .

The matrix  $C_s^g$  results directly from geographic to body DCM after incorporating static calibration values. This transformation generates a systematic error to be considered firstly, before going further into the treatment. We can notice that the model set up above is also valid for 2D line scanners when setting the horizontal angle  $\theta$  to zero.

As already mentioned, the estimation of standard deviation of attitude and position can be obtained from Kalman covariance matrix  $P_k$ , where  $k$  represents the interpolated time of each point of scan. Nevertheless, this will constitute a future field of work.

The error model associated to equations (11, 12) can be driven firstly from a linearization based on Taylor's

development theorem at an approximate value  $X_0$  applied on a function  $Y = f(X)$ :

$$Y = Y_{X_0} + \left(\frac{\partial Y}{\partial X}\right)_{X_0} \cdot \frac{X - X_0}{1!} + \left(\frac{\partial^2 Y}{\partial X^2}\right)_{X_0} \cdot \frac{(X - X_0)^2}{2!} + \dots + \left(\frac{\partial^n Y}{\partial X^n}\right)_{X_0} \cdot \frac{(X - X_0)^n}{n!} \quad (13)$$

Considering that the high-order terms have a negligible effect, the last formula becomes:

$$Y - Y_{X_0} \approx \left(\frac{\partial Y}{\partial X}\right)_{X_0} \cdot (X - X_0) \quad \text{or:} \quad v_Y \approx \left(\frac{\partial Y}{\partial X}\right)_{X_0} v_x$$

$$\text{And in a matrix form: } V_Y \approx J \cdot V_x \quad (14)$$

where  $J$  is the Jacobean matrix of  $Y$ ;  $v$  stands for a residual and  $V$  represents the matrix of residuals.

Assuming that the development takes place at a measured point  $P$ , we can detail the content of previous matrices:

$Y = (x_p^g \ y_p^g \ z_p^g)^T$  where  $Y = f(X)$  is given by equations (12).

$$X = (x_s^g \ y_s^g \ z_s^g \ \omega \ \phi \ \kappa \ \rho \ \varphi \ \theta)^T$$

$$V_Y = (v_{x_p^g} \ v_{y_p^g} \ v_{z_p^g})^T$$

$$V_x = (v_{x_s^g} \ v_{y_s^g} \ v_{z_s^g} \ v_{\omega_s^g} \ v_{\phi_s^g} \ v_{\kappa_s^g} \ v_{\rho} \ v_{\varphi} \ v_{\theta})^T$$

where  $\omega$ ,  $\phi$ ,  $\kappa$  are the Euler angles of  $C_s^g$ .

After linearization of equations (12), we obtain the Jacobean matrix of  $Y$  as following:

$$J = \begin{pmatrix} \frac{\partial x_p^g}{\partial x_s^g} & \frac{\partial x_p^g}{\partial y_s^g} & \frac{\partial x_p^g}{\partial z_s^g} & \frac{\partial x_p^g}{\partial \omega_s^g} & \frac{\partial x_p^g}{\partial \phi_s^g} & \frac{\partial x_p^g}{\partial \kappa_s^g} & \frac{\partial x_p^g}{\partial \rho_s^g} & \frac{\partial x_p^g}{\partial \varphi_s^g} & \frac{\partial x_p^g}{\partial \theta_s^g} \\ \frac{\partial y_p^g}{\partial x_s^g} & \frac{\partial y_p^g}{\partial y_s^g} & \frac{\partial y_p^g}{\partial z_s^g} & \frac{\partial y_p^g}{\partial \omega_s^g} & \frac{\partial y_p^g}{\partial \phi_s^g} & \frac{\partial y_p^g}{\partial \kappa_s^g} & \frac{\partial y_p^g}{\partial \rho_s^g} & \frac{\partial y_p^g}{\partial \varphi_s^g} & \frac{\partial y_p^g}{\partial \theta_s^g} \\ \frac{\partial z_p^g}{\partial x_s^g} & \frac{\partial z_p^g}{\partial y_s^g} & \frac{\partial z_p^g}{\partial z_s^g} & \frac{\partial z_p^g}{\partial \omega_s^g} & \frac{\partial z_p^g}{\partial \phi_s^g} & \frac{\partial z_p^g}{\partial \kappa_s^g} & \frac{\partial z_p^g}{\partial \rho_s^g} & \frac{\partial z_p^g}{\partial \varphi_s^g} & \frac{\partial z_p^g}{\partial \theta_s^g} \end{pmatrix} \quad (15)$$

Then, while passing from the residuals in expression (14) to the variances, the general law of propagation of variances is applied. Thus, we obtain the covariance matrix of the result  $Y$ :

$$\Sigma_{YY} = J \Sigma_{xx} J^T = \begin{pmatrix} \sigma_x^2 & \sigma_{xy} & \sigma_{xz} \\ \sigma_{xy} & \sigma_y^2 & \sigma_{yz} \\ \sigma_{xz} & \sigma_{yz} & \sigma_z^2 \end{pmatrix} \quad (16)$$

Where the elements of  $\Sigma_{xx}$  are the covariances of the scanner's position, attitude, range and angles described above.

The correlation between the scanner variables ( $\rho$ ,  $\varphi$ ,  $\theta$ ) and the navigation variables ( $x$ ,  $y$ ,  $z$ ,  $\omega$ ,  $\phi$ ,  $\kappa$ ) is inexistent. For a reason of simplification and as a preliminary assumption, we also set all the other non-diagonal values in the matrix  $\Sigma_{xx}$  to zero.

Hence, the resulting precision of 3D coordinates of a point can be extracted from the diagonal elements of  $\Sigma_{YY}$ . Also a global precision of the point can be expressed by the formula:

$$\sigma_{P_{3D}} = \sqrt{\sigma_x^2 + \sigma_y^2 + \sigma_z^2} \quad (17)$$

The interpretation of the linearized and derived form of equations (12) is rather complex. Indeed, the analysis of the influence of individual errors on the result cannot be done independently for each parameter. In this context, (Baltasvias, 1999) studied the effect of each variable successively on the resulting point coordinates by setting to zero the other parameters.

The diagonal elements  $j_{ii}$  of the product  $J^T \times J$  represent the mathematical contribution of each computation factor to the final accuracy, without taking into account its own variance. We will call each diagonal element “variable-coefficient” in the following paragraphs.

$$j_{ii} = (J^T \times J)_{(i,i)} = \left( \frac{\partial x_p^g}{\partial \alpha} \right)^2 + \left( \frac{\partial y_p^g}{\partial \alpha} \right)^2 + \left( \frac{\partial z_p^g}{\partial \alpha} \right)^2 \quad (18)$$

$i = 1, 2, \dots, 9$

$\alpha = x_s^g, y_s^g, z_s^g, \omega, \theta, \kappa, \rho, \varphi, \theta$  according to  $i$  value.

It could be proved that the effect of the variable-coefficient related to  $x_s^g, y_s^g, z_s^g, \rho$  is always linear, while the effect of the other variable-coefficients will be discussed and analysed later.

## 5. First tests, results and analysis

The test was carried out at the courtyard of INSA Strasbourg in suitable conditions of GPS reception, and we focused on the measure of one façade of the main building (20m high) at an average distance of 25 m. The travelled path was almost straight and plane. Our choice was to define a narrow acquisition window for capturing the point cloud with PointScape® (10° horizontally by a maximum value of 60° vertically). The angular resolution is set to 3 seconds of degree, for an average time of 2 minutes, and a total amount of 135000 points.

Figure 3 shows what a raw point cloud acquired by a mobile TLS system looks like. It is somehow a “compressed” scene of the scanned object.

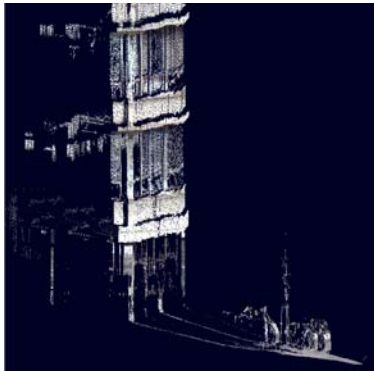


Figure 3. The raw point cloud

The treatment of this point cloud has been carried out in post-treatment mode according to equation (11) and is shown in Figure 4. The actual sampling ratio of GPS/INS integration is about 20 Hz while the scanner one is equal to 1600 points per second. Thus, an interpolation of GPS/INS measurements has to be done for each scanned point. We assume that the time interval between two consecutive points is the same whatever their position in the scanning sequence. Since the start time and scan duration are known, it is possible to interpolate linearly the time of each point of the cloud. Usually this stage is performed using Kalman filter, but it was not a priority in this first experiment, so a non-coupled mode of GPS/INS is used.

Equation (12) imposes having the vector of displacement and the rotation matrix for each point of the cloud. This task is time consuming and needs a particular programming solution for saving processor time.

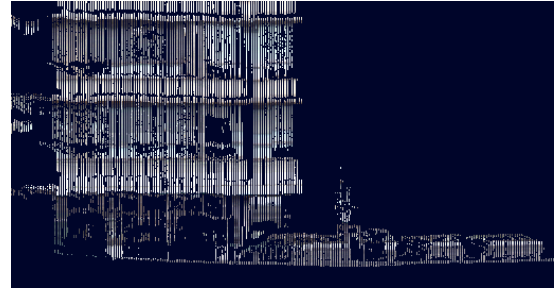


Figure 4. Georeferenced point cloud

The actual point cloud is still affected by poor synchronisation between the system components, but this error is not developed in this first experiment, since for the time being our system is still under test.

In order to compute the error budget of our system, individual errors for the different components mentioned in the previous paragraph have to be estimated. The quality of GPS observations driven from the coordinate’s variance-covariance matrix is estimated in LEICA Geo Office®. It is equal to 4.8 mm in the horizontal plane and 9.8 mm for 3D positioning quality when the total ambiguity is resolved. The GPS acquisition frequency was 1 point/sec. The INS observation quality is set to  $\pm 0.2$  deg/sec for the triplet of angles. INS quality is obviously lower than the GPS one and its influence is remarkable on the final point cloud. The TLS quality obtained from calibration according to Trimble® test is mentioned in part 2.

The individual errors for the different components given previously are considered to be the same for all the points. Table 1 shows the set of points used as test sample and their observations. They have been chosen as well distributed in navigation and in the point cloud. Geographic coordinates of the scanner origin are not given, because they have no effect in the error propagation stage.

N	$\omega^\circ$	$\phi^\circ$	$\kappa^\circ$	$\rho$ (m)	$\varphi^\circ$	$\theta^\circ$
1	0	0	0	30	20	5
2	0.5	0.5	3	30	20	5
3	5	5	10	30	20	5
4	-5	-5	-3	30	20	5
5	2	2	5	30	20	5
6	0	0	10	10	20	5
7	0	0	0	30	38	5
8	2	2	5	30	-20	-5
9	5	5	3	20	0	0
10	0.5	2	5	30	20	1

Table 1. Sample of 10 points and their observation parameters.

Based on equations (16) and (17), we obtain:

N	$\sigma_{x_p^g}$ (m)	$\sigma_{y_p^g}$ (m)	$\sigma_{z_p^g}$ (m)	$\sigma_{P3D}$ (m)
1	0.037	0.100	0.900	0.145
2	0.038	0.104	0.990	0.140
3	0.037	0.099	0.100	0.147
4	0.019	0.068	0.068	0.098
5	0.065	0.088	0.099	0.140
6	0.024	0.029	0.034	0.055
7	0.065	0.104	0.080	0.149
8	0.043	0.104	0.097	0.149
9	0.009	0.070	0.700	0.099
10	0.034	0.100	0.099	0.140

Table 2. Computed variances of x, y and z.

We can observe a global precision of about 15 cm while points having realistic range values ( $\rho$  is about 30 m) are taken into consideration. This effect can be explained by the non-coupled mode for GPS/INS integration which does not enhance any of their precisions. The linear relation between the range and the global point accuracy can be noted easily (e.g. point 6 with lowest range value  $\rho$ ). Moreover, one can notice the low error observed on the  $x$  axis which was roughly parallel to the displacement direction.

These outcomes are confirmed when representing the variable-coefficients of equation (18) graphically (see Figure 5). Only the variable-coefficients related to the five angles ( $\omega$ ,  $\phi$ ,  $\kappa$ ,  $\varphi$ ,  $\theta$ ) are represented herein because of their comparable coefficients.

The weak effect of the variable-coefficients of  $\omega$  on the 3D precision is seen whatever the INS accuracy.

The scan vertical angle ( $\varphi_{max} = 38^\circ$ ) has a high contribution of the accuracy of point 7. Thus, coupling this effect with the one of the range  $\rho$  generates a non-homogeneous precision on the scanned facades, especially on the high parts.

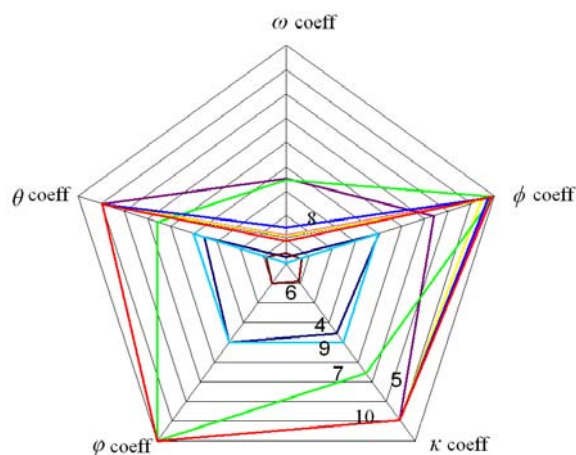


Figure 5. Variable-coefficient of ( $\omega$ ,  $\phi$ ,  $\kappa$ ,  $\varphi$ ,  $\theta$ ) for 10 points

Such results can be verified either by direct point measurement using conventional tachymetric methods or by rescanning the same facade in a static mode. In the last case, the shift and the rotation resulting from ICP method of consolidation could stand for a good index for accuracy estimation.

## 6. Conclusion and future research

In this paper, a prototype of mobile mapping system based on TLS was presented. Although the experimental results obtained so far are not sufficient, we can consider that the minimum required hardware and software has been defined. It has proved to be a solid basis for future experiments. The error analysis has also been introduced and has led to the expression of the total precision of 3D points. Thus, the final error model permits to estimate the quality of the processed point cloud. The main purpose of this work was to set out and initialize the system operation requirements and to provide first results which will be the starting point of further experiments. Particularly, we intend to improve drastically the synchronisation issues. We hope to reach acceptable results in the near future suitable for large and medium scale urban mapping, while for fine scale models an additional attention must be paid especially to GPS/INS integration.

## REFERENCES:

### References from Journals:

Baltsavias, E.P., 1999. Airborne laser scanning: basic relations and formulas. *ISPRS Journal of photogrammetry & remote sensing* 54, pp. 199-214.

Bar-Itzhack, I.Y. and Berman, N., 1988. Control theoretic approach to inertial navigation system. *AIAA Journal of Guidance, Control & Dynamics*, vol. 11, pp. 237-245.

Benson, D.O., 1975. A Comparison of Two Approaches to Pure-Inertial and Doppler-Inertial Error Analysis. *Aerospace and Electronic Systems, IEEE Transactions on: Volume: AES-11*, Issue: 4, pp. 447-455.

Wang, J., Lee H.K., Hewitson, S. and Hyung-Keun L., 2003. Influence of Dynamics and Trajectory on Integrated GPS/INS Navigation Performance. *Journal of Global Positioning Systems* Vol. 2, No. 2, pp. 109-116.

Kong, X., 2004. INS algorithm using quaternion model for low cost IMU. *Robotics and Autonomous Systems*, Volume 46, Issue 4, pp. 221-246.

### References from Books:

Reshetyuk, Y., 2006. Investigation and calibration of pulsed time-of-flight terrestrial laser scanners, Department Transport and Economics, KTH publication, pp 39-80.

### References from other Literature:

Abuhadrous, I., Nashashibi, F., Goulette, F., Laugeau, C., Ammoun, S., 2004. Digitizing and 3D Modeling of Urban Environments and Roads Using Vehicle-Borne Laser Scanner System", *IEEE/RSJ Int. Conf. on Int. Robots and Systems*, Sendai, Japan.

Lichti, D.D. and Licht, M.G., 2006. Experiences with terrestrial laser scanner modelling and accuracy assessment. *Proceedings of the ISPRS Commission V Symposium 'Image Engineering and Vision Metrology*. Dresden Germany

Rankin, J., 1994. An error model for sensor simulation GPS and differential GPS, *Position Location and Navigation Symposium*, IEEE, Las Vegas, NV, pp. 260-266.

Stovall, S. H., 1997. Basic Inertial Navigation. Report NAWCWPNS TM 8128, Naval Air Warfare Center Weapons Division California, USA.

Wang, J., Wang, J.J., Sinclair, D, and Watts, L., 2006. A neural network and Kalman filter hybrid approach for GPS/INS integration. *12th IAIN Congress & 2006 Int. Symp. on GPS/GNSS*, Jeju, Korea, pp. 277-282.

Zhao, H., Shibasaki, R., 2001. High accurate positioning and mapping in urban area using laser range scanner, *Proceedings of IEEE Intelligent Vehicles Symposium*. National Institute of Informatics, Tokyo, Japan, pp. 125-132.